Zonal Detached Eddy Simulation of the Fan-Outlet Guide Vanes Stage of a Turbofan Engine: Part I-Methodology, Numerical Setup, and Aerodynamic Analysis

Benjamin François, Cyril Polacsek, Raphaël Barrier

Journal of Turbomachinery. Received July 06, 2021;
Accepted manuscript posted May 04, 2022. doi:10.1115/1.4054528

Zonal Detached Eddy Simulation of the Fan-OGV Stage of a Turbofan Engine: Part I - Methodology, Numerical Setup and Aerodynamic Analysis

Benjamin François*
ONERA,
The French Aerospace Lab
DAAA†
Helicopter, Propeller
and Turbomachinery Unit
8 rue des Vertugadins
92190 Meudon, France

Cyril Polacsek
ONERA,
The French Aerospace Lab
DAAA
Numerical Aeroacoustic Team
29 Avenue de la Division Leclerc
92320 Châtillon, France

Raphaël Barrier,
ONERA, The French Aerospace Lab
DAAA
Helicopter, Propeller and Turbomachinery Unit
8 rue des Vertugadins
92190 Meudon, France

ABSTRACT

The present article deals with the Zonal Detached Eddy Simulation of the fan module of a modern turbofan engine for the prediction of the broadband noise due to the interaction of the fan turbulent wakes with the stationary outlet guide vanes. The simulation relies on a hybrid RANS/LES approach with a zonal strategy: the core airflow is treated in RANS while the bypass airflow is solved with the hybrid approach. The simulation was performed during four revolutions and statistical convergence was reached. Inspections of the flow-fields

*Address all correspondence to this author : benjamin.francois@onera.fr
†Aerodynamics, Aeroelasticity, Acoustics Department

highlight a consistent behaviour of the shielding function (border between RANS and LES solving areas) around the blade walls and at the trailing-edge for a such complex flow. The fan module was tested in the AneCom facility in which hot-wire measurements were made in-between the fan and the outlet guide vanes. The numerical results are compared to this large dataset of measurements. The flow maps are well retrieved by the simulation for both the time-averaged and the turbulent quantities. Comparison of radial profiles shows an excellent agreement for the three RMS component of the velocities between ZDES and the measurements, particularly in the tip gap flow area, in which RANS results do not reproduce correctly the flow quantities. The wake shape, a key feature in the mechanism of generation of rotor-stator interaction noise), is quite well predicted by the ZDES simulation. These numerical results demonstrate the maturity of the approach for the simulation of complex turbomachinery flows.

1 INTRODUCTION

Because of the significant reduction of tonal noise in modern turbofans, the broadband component of the overall perceived noise has become a growing contribution and is nowadays a major topic of concern for aircraft engine manufacturers [1]. The present work adresses a hybrid RANS/LES methodology to predict this noise contribution on a fan module of a civil modern turbofan at approach conditions. Only the aerodynamic simulation and the associated results are presented here, the broadband noise analyzes are discussed in a complementary (Part II) paper [2]. In the fan module, a major contribution of the broadband noise is the interaction of the turbulent structures generated in the fan wakes with the outlet guide vanes (OGV) located downstream [3]. The turbulent structures are scattered by these vanes which generate radiating acoustic waves in the upstream and downstream directions.

Because of the high Reynolds number involved (around one million), turbulence scale resolved simulations of a fan blade or a fan stage of a turbofan engine require a significant computational effort. For this reason, such simulations remain scarce in the literature. Indeed, the high Reynolds number implies tremendous mesh refinement in the boundary layer for Wall-Resolved Large Eddy

Simulations (WRLES). In Wall-Modeled LES (WMLES), the use of wall law enables to reduce the computational effort compared to WRLES but the mesh requirement still strongly increases with the Reynolds number. An alternative way is to resort to hybrid RANS/LES approaches in which the whole boundary layer is solved with a RANS modeling. Hence, their numerical cost is much less dependent on the Reynolds number. This simulation strategy is followed here and relies on the Zonal Detached Eddy Simulation from Deck *et al.* [4]. This approach has already been used by Bonneau *et al.* [5] on a turbofan for the prediction of broadband noise in which only a fan blade was simulated. Aerodynamic features of the wake were extracted (wake width, velocity deficit, turbulent kinetic energy) to feed an Amiet-like code to compute the noise radiating by the OGV. François *et al.* [6] extended the work of Bonneau *et al.* by performing simulations of the fan blade with the outlet guide vanes, giving access to the unsteady pressure fluctuations on the vanes. The acoustic predictions of these simulations were presented in a dedicated conference paper by Polacsek *et al.* [7].

To the authors' knowledge, previous works relying on turbulence scale resolved simulations for aeroacoustic of turbofans were performed mainly on the NASA Source Diagnostic Test (SDT) configuration with different numerical approaches: WRLES (Kholodov *et al. [8]*), WMLES (Leonard *et al.* [9], Arroyo *et al.* [10], Hah and Romeo [11]), hybrid RANS/LES (Shur *et al.* [12], Suzuki *et al.* [13]) and Lattice Bolzmann method (Casalino *et al.* [14]). The present turbofan configuration (ACAT1 fan stage) treated in this paper is quite new in the literature [15–17] and only a few partners from the associated project performed turbulence scale resolved simulations (Lewis *et al.* [18], Tucker and Wang [19]).

The present paper is the continuation of the work from François *et al.*, Polacsek *et al.* [6, 7]: a new Zonal Detached Eddy Simulation was performed accounting for a more realistic boundary layer upstream of the fan, the turbulence scale-resolved area was slightly extended and the outlet pressure in the bypass airflow was adjusted to reduce the massflow rate discrepancy with the measurement. Also, a large dataset of measurements including the final calibrations and the uncertainties, not present in the conference papers, are presented and compared to the numerical results. RANS results are also included in the comparison. The paper is organized as follows.

First, the paper presents the main features of the fan geometry and operating point. Then, several aspects of the CFD strategy such as the methodology, the mesh critera, the boundary conditions and the numerical parameters are discussed. Third, analysis of the convergence of the simulation are addressed. Fourth, three-dimensional analysis of the flow inspecting the consistency of the ZDES solution are carried out. Finally, comparisons with hot-wire measurements performed in AneCom test falicity [15] are discussed.

2 PRESENTATION OF THE CONFIGURATION

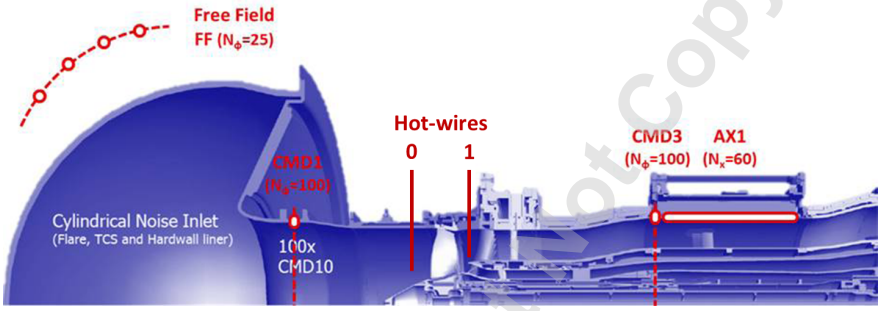

Fig. 1. Sketch of the rig set-up at AneCom's UFFA (reprint with TurboNoiseBB Consortium permission) with the hot-wire probes.

The turbofan configuration is the ACAT1 fan stage which was studied in the framework of TurboNoiseBB project (2017-2020), an EU-funded[1] H2020 project. Main objectives of this project were dedicated to the improvements of the measurements techniques and numerical methods for the prediction of broadband noise on modern turbofan. The test-rig in which hot-wire and acoustic measurements were carried out is depicted in Fig. 1. The specificity of this configuration is the short inter-stage distance (roughly equal to one fan chord). The turbofan is equipped with 20 fan blades and 44 outlet guided vanes (OGV) and studied at rig-scale (the outer radius of the fan is $0.42\ m$). Because the bypass ratio is around six, the rotor-stator interaction (RSI) with the Inlet Guide Vanes (IGV) in the primary airflow can be assumed negligible compared to the bypass RSI contribution. As a result, the IGV are not accounted for in the simulation. The configuration is studied at the approach conditions ($\Omega = 3828.4\ rpm$, $M_{tip} = 0.57$) for which the RSI noise is

[1] EU: European Union

dominant, as outlined by Envia *et al.* [20] and Casalino *et al.* [14].

3 METHODOLOGY

3.1 Zonal Detached Eddy Simulation

The Zonal Detached Eddy Simulation (ZDES) developped by Deck [4] and implemented in the elsA code [21] is used here. This formulation offers the possibility to treat different parts of the computational domain with a specific ZDES formulation or a full URANS solving. This approach has already been used on aircraft, space launchers, jet flows and turbomachinery [5, 22, 23]. The zonal aspect enables to alleviate the computational cost compared to other DES techniques with areas treated with a RANS solving, requiring a reduced mesh density. Also, such approach offers a large flexibility for the user to choose the most suitable ZDES formulation with respect to the flow physics to deal with. The present paper only describes the ZDES mode 2 (refering to Deck *et al.* [4]) used in the simulation and the reader can refer to the aforementioned paper for further information.

The ZDES mode 2 allows the boundary layer to be solved with an URANS treatment, the remaining part being treated by a LES solving with an automatic detection of both areas. To know whether the computed cell is in the attached boundary layer or not, a shielding function f_d, inherited from the Delayed Detached Eddy Simulations (DDES) from Spalart *et al.* [24], is evaluated. It reads:

$$r_d = \frac{\nu + \tilde{\nu}}{\sqrt{U_{i,j}U_{j,i}}\kappa^2 d_w^2}, \quad f_d = 1 - tanh\left(8r_d\right)^3$$

where $\tilde{\nu}$ is the eddy viscosity solved in the equation of the Spalart-Allmaras turbulence model [25][2], ν the molecular viscosity, $U_{i,j}$ the velocity gradient, κ the Karman constant, d_w is the distance to the wall. The parameter r_d is equal to one in the logarithmic area of the boundary layer and vanishes at the edge of the boundary layer. Consequently, the function f_d equals zero in the boundary layer and activates the URANS mode. Outside the boundary layer, it equals one and allows the switch

[2] In the classic DDES from Spalart *et al.* [24], the variable ν_t is used.

to the LES mode. The ZDES mode 2 from Deck *et al.* presents similarities with the DDES from Spalart *et al.* [24]. The main difference concerns the choice of the characteristic mesh length. In DDES, it is based on the largest cell size such as $\Delta = \max(\Delta x, \Delta y, \Delta z)$ while in ZDES, it reads:

$$\Delta = \begin{cases} \Delta_{max} = \max(\Delta x, \Delta y, \Delta z) & if\ f_d < f_{d0} \\ \Delta_{vol} = (\Delta x \Delta y \Delta z)^{1/3} & if\ f_d > f_{d0} \end{cases}$$

where f_{d0} is a constant equal to 0.8. Deck *et al.* made comparisons between the DDES and the ZDES mode 2 on various applications (mixing layer, backward facing step, airfoil). They highlight that ZDES keeps the strong assets of DDES such as the treatment of the attached boundary layer while improving other aspects such as reducing the delay in the formation of the instabilities.

3.2 Flow Domains

3.2.1 Repartition of RANS and ZDES zones

The objective being the simulation of the interaction between the fan wake with the OGV in the bypass airflow, the core airflow can be solved with an URANS solving, reducing the mesh requirements in this area. Also, the upstream turbulence rate measured in the experimental facility upstream of the fan is very low (around 0.3%) [15]. Hence, the noise associated with the impingement of the infinite inflow turbulence on the fan is negligible compared to the RSI noise. Thus, an URANS modeling is sufficient upstream of the fan. All the remaining areas of the computational domains are treated with the ZDES formulation described in section 3.1. The border between the URANS domain and the ZDES mode 2 domain must be chosen with care at the separation between the primary and the bypass airflow. Indeed, the ZDES mode 2 domain needs to be large enough to ensure that the flowpaths nearby the fan blade, going then into the bypass airflow and generating wakes, are well treated in ZDES mode 2. Otherwise, part of the fan wakes interacting with the OGV will be solved in RANS and they will remain RANS-like in the bypass airflow domain. An illustration of the RANS/DES zones on single channel computational domain is given in Fig. 2.

Journal of Turbomachinery. Received July 06, 2021;
Accepted manuscript posted May 04, 2022. doi:10.1115/1.4054528

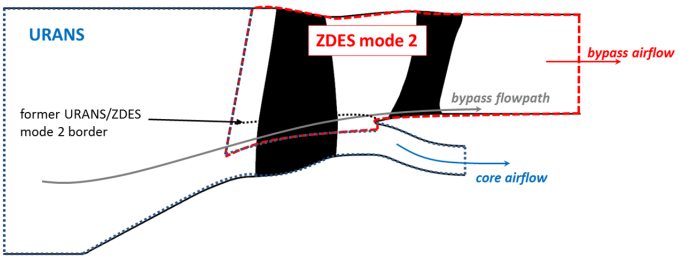

Fig. 2. Repartition of the RANS and ZDES mode 2 areas in the computational domain. The border between URANS and ZDES mode2 area from the former simulation [6] is indicated. The borders of the present simulation are shown with blue and red colors.

3.2.2 Modification of the geometry

Motivation To reduce the numerical cost, only a few interblade channels are simulated. The current number of blades (20 for the fan, 44 for the OGV) is unfavorable to reduce the computational domain to a few inter-blades channels. For unsteady RANS simulations, classic phaselag boundary conditions allows the reduction to one channel. Because they are currently based on the usual Fourier decomposition, they are unadapted for the convection of broadband structures. Consequently, a more favorable option is to change the blade number of the OGV to get a suitable divisor and allow the use of periodic boundary conditions instead. Even if the periodicity is still questionnable for the turbulence structures between adjacent channels, the spectral content is believed to be conserved through these periodic boundary conditions. This strategy has already been justified and used by several authors on the NASA SDT for broadband noise predictions [9–11]. The same strategy was followed on the ACAT1 configuration by Lewis *et al.* [18] for WMLES.

OGV Rescaling and aerodynamic impact The number of the OGV is thus reduced from 44 to 40. To keep the same flow pattern, the solidity is kept constant meaning that the chord is increased by 10%, the leading-edge position is unchanged. Such a blade number modification allows to reduce the computational domain to one fan channel and two OGV channels. The unchanged geometrical parameters are the solidity, the leading-edge position, its sweep and lean angles, the thickness-to-chord and angles law along the streamwise variable and inner and outer duct walls. The modified parameters with respect to the original geometry are the number of blades (44 to 40), the chord ($+10\%$), the aspect ratio and the thickness.

RANS simulations of the fan-OGV configuration with the nominal number of OGV and with the modified number of rescaled OGV were performed at the same massflow by François *et al.* [6]. Inspection of the absolute flow angles, absolute Mach number at position upstream and downstream of the OGV show identical radial evolution. Same conclusions were drawn regarding the pressure maps distribution on the walls. The conservation of the solidity is a key aspect in the OGV modification. First, it enables to get a similar mean velocity field to convect the fan wake through the vanes. Second, a modification of solidity can affect the vane aeroacoustic response due to wake interaction, as shown by Posson *et al.* [26].

3.2.3 Computational domain

The computational domain is composed of one fan and two OGV inter-blade channels. The fan and the OGV domains are solved in their respective frame of reference. The inlet of the computational domain is located at four fan chords upstream of the fan leading-edge while the outlet is located at three vane chords downstream of the vane trailing-edge.

3.3 Boundary Conditions

The modification of the OGV geometry mentioned in the previous section enables to get the same azimuthal periodicity with one fan blade and two vanes. As a consequence, periodic boundary conditions can be used for the azimuthal border of the computational domain for the unsteady simulation. At the interface between the rotating domain of the fan and the fixed domain of the vanes, a sliding mesh treatment is performed. It relies on interpolation of the state vector of a donor grid on a receive grid and then on a half-sum between the donor and the receiver cells from both domain on the conservative variables. Errors of interpolation on a few cells between the moving grids were detected by Polacsek *et al.* [7], generating spurious noise sources. Corrections were brought in the *elsA* flow solver in the moving grid BC treatment and these interpolations errors have now fully disappeared in the ZDES simulation presented in this paper and the companion paper dedicated to the acoustic analysis.

At the inlet of the computational domain, stagnation pressure, stagnation enthalpy and absolute velocity directions are imposed. For the outlet of the core and the bypass airflow, a radial

equilibrium is imposed with a user-prescribed pressure at the lower wall. The inlet and outlet BC are combined with sponge layer to limit spurious reflections (see further details in Sec. 3.4.2).

Compared to the ZDES performed by François *et al.* [6], two modifications were brought in the simulation to better match the experimental conditions:

- A radial heterogeneous profile of stagnation pressure (instead of an uniform one) is imposed at the inlet of the present simulation to match the hot-wire measurements upstream of the fan (see Fig. 3-a). The shroud boundary layer impinging the fan has a significant effect on the tip gap flow. With this radial profile, the present ZDES is thus more realistic than the previous one. Axial velocity profile (Fig. 3-b) highlights a quite good agreement with the measurements, with discrepancies lower than 2 m/s.
- The user-prescribed pressure at the bypass lower wall was slightly increased to better match the measured massflow rate. Discrepancies between measured and simulated massflow rates reduce from $+1\%$ to -0.25%. Because the operating point is close to surge, these differences may have a significant influence on the shape of the wakes and tip gap flows impinging the OGV. Furthermore, flow separation are observed on both fan and OGV, with significant effects on acoustic radiation, as discussed in the companion paper [2].

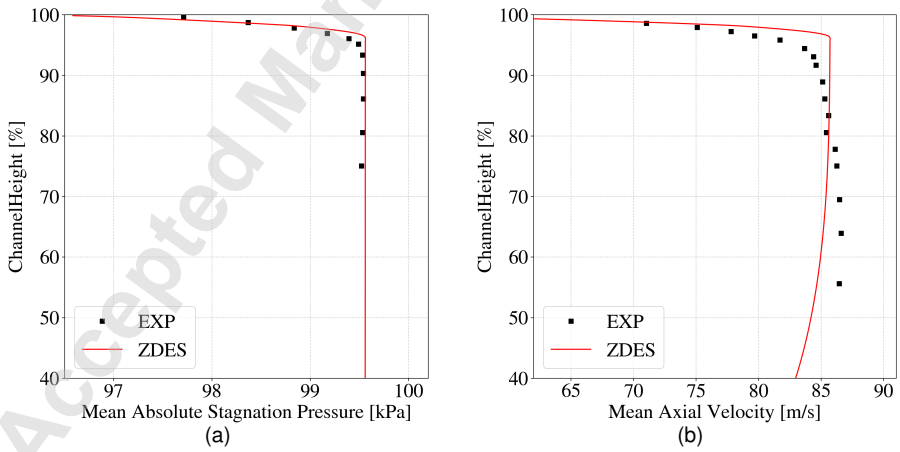

Fig. 3. Comparison of the absolute stagnation pressure (a) and the axial velocity (b) between the hot-wire measurements and the simulation upstream of the fan (position 0)

3.4 Mesh

3.4.1 Mesh criterion

Two sets of criteria were used to build the present mesh. The first relies on internal best practices concerning the use of the ZDES mode 2. The cell size verifies $\Delta x^+,\ \Delta y^+,\ \Delta z^+ < 200$ in the free shear flow areas, namely a cell size lower than $0.6\ mm$ for the present mesh. The first wall mesh size verifies $\Delta y^+ \leq 1$.

The second criterion relies on the aeroacoustic mechanism at stake. The impinging turbulent wake from the fan blade can be modelled by a set of hydrodynamic waves. The impingement of each hydrodynamic wave, also called gust, on the vane generates acoustic waves with the same frequency. Among the different waves at stake and given the Mach number of the considered flow, the gust wavelength is here the most stringent. Its expression reads $\lambda_h = U_c f^{-1}$ where U_c is the local convection speed and f is the frequency. Preliminary RANS simulations show that in the interstage area, the absolute velocity ranges from $100\ m/s$ and $140\ m/s$. Accounting for the smallest velocity value and sampling the wavelength by 20 points leads to a mesh size of 0.25 mm at 20 kHz, (human ear upper limit frequency). Such cell size would imply for the intended computational domain a mesh of 3 billions cells. An acceptable trade-off between cost and accuracy is to select a cell size of 0.5 mm, leading to a mesh of 1/8 of this grid size (e.g. 400 million cells) while ensure a sampling of 20 points at 10 kHz.

3.4.2 Mesh characteristics

Repartition of points Build following the criteria mentionned above, the mesh has a total cell number equal to 380 millions. The mesh used is structured and multi-blocks. Its first mesh size is three micrometers and corresponds to y^+ values equal to 1 at the cell center. Its main characteristics are gathered in Fig. 4 and sectional views are given in Fig. 5.

Buffer areas Near the inlet and the outlet, damping zones with stretched cells in the axial direction are used to avoid numerical reflections on the boundary conditions. Their expansion ratio remains lower than 1.2 to prevent additional spurious acoustic reflections from unsuited grid transitions. The largest cell size upstream of the fan is three centimeters while it is equal to two

Number of points for one channel	FAN domain	OGV domain
Blade-to-blade area		
Azimuthal direction	380	264
Streamwise direction from LE to TE	280	400
From blade to the moving grid interface area		
Azimuthal direction	300	160
Streamwise direction	248	160
Radial direction	771	625
Primary airflow	85	
Splitter	41	
Secondary airflow	645	
Tip gap (radial direction)	45	
Total (million)	180	100

Fig. 4. Repartition of points of the mesh

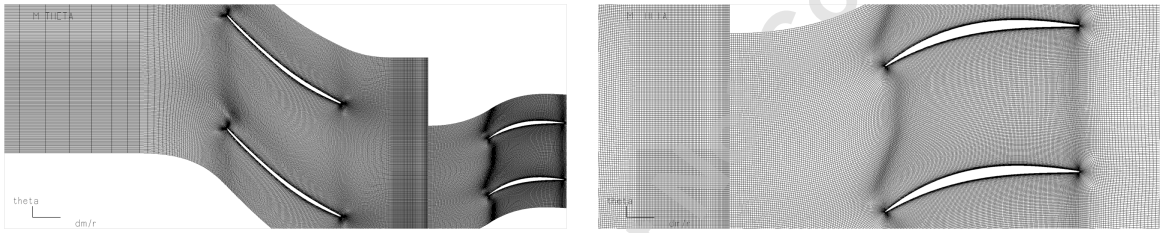

(a) Fan inter-blade channel (b) Vane inter-blade channel

Fig. 5. Blade-to-blade view at mid-height of the OGV span. Meshes with one point over two are shown in the pictures.

centimeters downstream of the OGV.

3.5 Flow Solver and Numerical Parameters

The flow solver is the elsA software [21], developed at ONERA. This compressible flow solver is based on a cell centered finite volume technique and structured multiblock meshes. The time scheme is achieved by an implicit second order scheme based on a Newton algorithm. The timestep has been set to $3.2 \times 10^{-7} s$. The choice was mainly driven by acoustic CFL[3] number considerations and computational cost (the selected timestep is small enough to capture the turbulent structures at stake). It corresponds to a convective CFL number around 36 in the smallest cells in the boundary layer and of 0.35 for cells the length of which is 0.5 mm. This timestep samples the fan blade passing periods by 2400 and the revolution by 48000. 5 sub-iterations are used in the inner-loop of the time scheme and the residuals decrease by one order of magnitude.

[3] Courant Friedrichs Lewy

The convective flux discretization is treated with the AUSM (Advection Upstream Splitting Method) scheme with a third order limiter. The turbulence model used is the Spalart-Allmaras model [25]. The simulation was performed on the supercomputers from CINES[4]. The simulation is done on 28 nodes and 672 cores, the total computational time is 2 million of CPU hours. Nearly four full revolutions were simulated.

3.6 Time Convergence

3.6.1 Initialization setup and Numerical transient

To reduce the numerical transient in the ZDES, a preliminary set of RANS and then URANS simulations were performed. The URANS simulation was run until the massflow rate was converged, namely two complete revolutions.

The time-length of the numerical transient is here determined by the convergence of the time-averaged quantities (over a large time-width with respect to the blade period) of the flow quantities either global (massflow) or local (axial momentum on a numerical probes). Figure 6 gives an illustration by showing the evolution of the bypass air mass flow non-dimensioned by its final value[5] at $t = 76$ FBP[6]. Both the instantaneous signal and the time-averaged one over ten FBP are shown. The abscissa axis is given in fan blade passage (20 equals a complete revolution). From the URANS simulation, the massflow shifts slighly because of the flow solution is quite different between the RANS and the ZDES in the flow separated areas. The massflow curve shows that the massflow is stabilized after two revolutions (variations of the time-averaged quantity on ten fan blade passages are lower than 0.2%). Flow quantities such as the axial momentum and the static pressure on numerical probes (not shown here for conciseness) meet the same requirement. The conjoint analysis of different time-averaged flow quantities indicates that the numerical transient lasts two revolutions.

[4]French National Computing Center
[5]This nondimensionalization gives direct access to the time-variation of the signal in percent.
[6]FBP:Fan Blade Passage

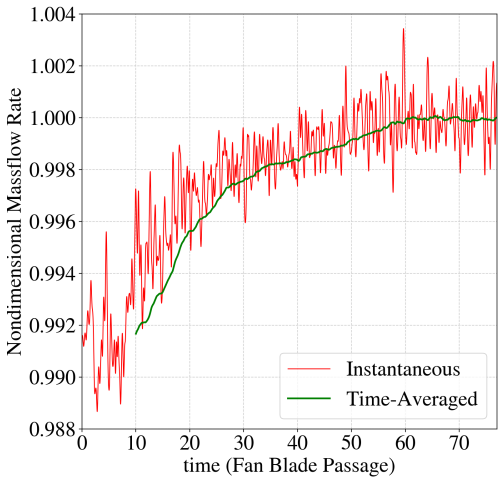

Fig. 6. Convergence of the bypass air massflow rate at the outlet of the computational domain, nondimensioned by the massflow rate at t=76 FBP (Fan Blade Passage).

3.6.2 Statistical convergence

For the convergence of the statistics, the numerical transient of the signal is removed from the complete signal. Only the portion from $t = 40$ FBP to $t = 76$ FBP is used to perform the statistics. Because the flow quantities exhibits strong deterministic signatures due to fan-OGV interaction in both the fan and the OGV computational domain, a cyclostationnary (or phase-averaged) decomposition of the signal is used. Inspired by the pioneer idea of Hussain and Reynolds [27], the signal is split into a deterministic and a stochastic part $u(x,t) = u_{cyclo}(x,t) + u_{stoc}(x,t)$ where $u_{cyclo}(x,t)$ contains the deterministic variation of the signal and its time averaging and $u_{stoc}(x,t)$ the remaining part of the turbulent signal. The cyclostationnary signal $u_{cyclo}(x,t)$ is calculated with the number of fan blade passages equal to $N(t) = E\left(T_{BP}^{-1}(t-t_0)\right)$ where E is the floor function, T_{BP} is the period of one blade passage and t_0 is the duration in time of the numerical transient. This relation enables to see the progressive convergence of the cyclostationnary signal. The last period of the cyclostationnary signal is then used to compute the fluctuating part. In the fan domain, the OGV blade passage period is used while in the OGV domain, the fan blade passage period is used.

A direct application is performed on the axial momentum signal on the numerical probe located at 90% of channel height near the OGV leading-edge. Figure 7 presents the instantaneous signal

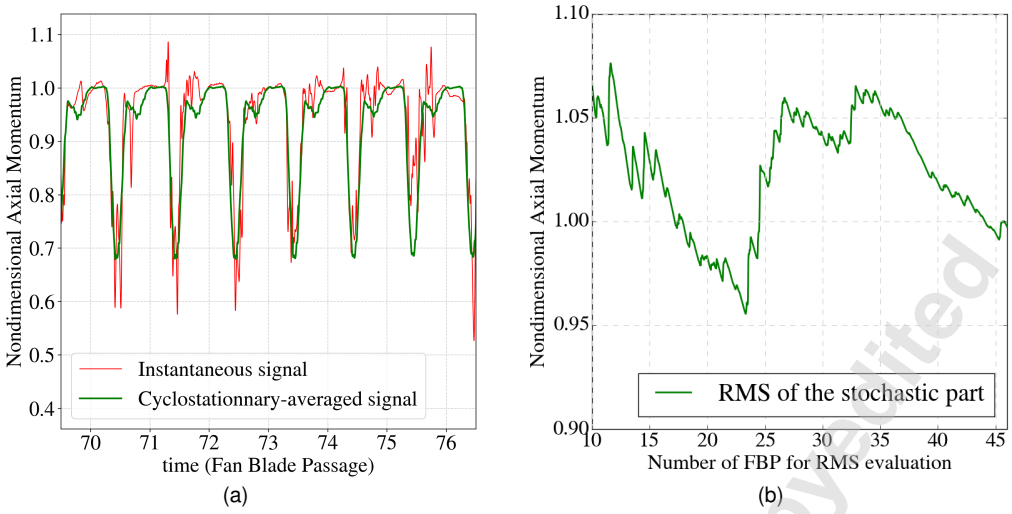

Fig. 7. (a) Instantaneous and cyclostationnary signals of the axial momentum on a numerical probe at 90% of channel height, near the OGV leading-edge. Wake and part of the tip gap flow can be seen respectively large and small axial momentum dips, (b) Deviation of the RMS evaluation of the stochastic part of the same probe signal over a given number of FBP with respect to the RMS value of the full signal.

during six FBP and the cyclostationnary signal. In the cyclostationnary signal, the stochastic part of the signal is filtered. The identical shape of this signal between the successive fan blade periods indicates that the signal is phase-averaged. Accurate repeatability of the phase-averaged FBP signatures is a good indicator of the convergence of the periodic contributions to be assessed in view of cyclostationnary analyses. In contrast, the instantaneous signal exhibits different velocity deficits for each fan blade period due to the stochastic nature of turbulence.

The phase-averaged property of the signal indicates that the time signal (without the numerical transient) is long enough to get converged cyclostationnary averages and thus reliable informations for the acoustic prediction presented in the companion paper. The turbulent signature used for broadband noise analyzes is assessed by subtracting the cyclostationnary part to the instantaneous signal. The convergence of this part of the signal is studied in Fig. 7-b : the Root Mean Square (RMS) is calculated over several numbers of FBP and deviations with the RMS evaluation are evaluated. It shows that for this numerical probe within the tip gap flow, the RMS estimation is converged with an accuracy of 5%. Lower RMS convergence levels (2%) are found on other numerical probes at mid-height, not shown here for conciseness.

4 VERIFICATION OF ZDES

This section focuses on the analysis of the aerodynamics flow-field and on the consistency of the flow solution obtained with the ZDES approach.

4.1 Zonal solving

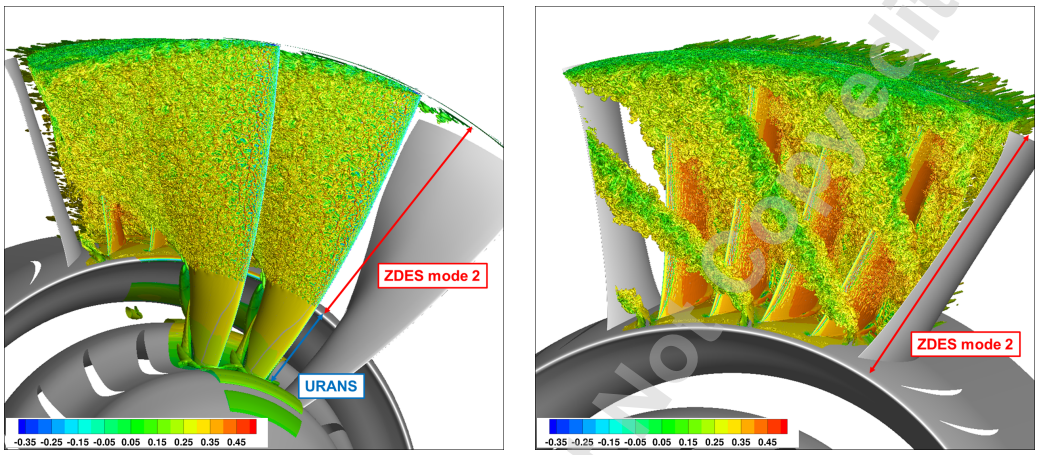

Fig. 8. Illustration of the zonal solving with ZDES by the visualisation of iso-value surfaces of the Q criterion ($\overline{Q}$=10 with $\overline{Q}$=$Q\times t_{adim}^2$ and t_{adim}=2.915 ms) around the fan blades (a) and around the OGV blades (b). The color indicates the non-dimensioned axial momentum (ρ_{adim}=1.185 kg/m^3 and V_{adim}=343.0 m/s).

Figure 8 presents a visualization of the instantaneous flow-field around the fan blade: surfaces of iso-values of the Q criterion colored by the axial momentum are displayed. It illustrates the zonal solving with the ZDES. The core airflow is treated in URANS and only very large turbulence structure are present such as an horseshoe vortex at the intersection of the fan blade and the hub. The bypass airflow is treated with the ZDES mode 2 (see Section 3.1). Because the flow separates at the leading-edge of the fan for this operating point, turbulent structures are generated there and are convected downstream. Figure 8 illustrates also a benefit of the ZDES approach: thanks to the reduced mesh effort in the boundary layers, a high grid density (cell width of 0.5 mm) could be used in the free-shear areas allowing the capture of very small turbulent structures. Such mesh density in these areas would require a larger number of cells in the whole mesh with a WMLES approach.

4.2 Convection of the fan wakes through the OGV

The main source of broadband noise is the interaction of the turbulent structures from the fan wake with the OGV walls. An important key point in this simulation is to ensure that the turbulence is properly convected from the fan through the OGV. Figure 9 presents fields of vorticity magnitude on a developed blade-to-blade surface. The vorticity fields are consistent: the fan wakes are convected without noticeable attenuation or numerical artefact through the stage interface and the periodic boundary conditions. Fig. 8-b gives a hub-to-shroud view of the fan wakes interacting with the OGV, supporting the previous statement.

Figure 9 depicts in thick black lines the areas in which the shielding function f_d equals 0.95, defining thus the border between the RANS solving (in the boundary layer) and the LES solving (in the free shear flow areas). For both fan and OGV blades, this RANS solving is consistent and seems qualitatively to encompass the whole boundary layer. A noticeable point is the rapid switch from RANS to LES at the trailing-edge of the blade (visible in the zoom in Fig. 9). The RANS boundary layer velocity profile degenerates into turbulent eddies due to a good detection of a free-shear flow area and the specific features of the ZDES described in the work of Deck *et al.* [4]. Similar conclusions with the same approach were drawn by Gand on a flow separation on a spoiler [28] and Verrière *et al.* on a jet flow [29].

A second noticeable point concerns the shielding function shape around the OGV walls: the interaction of the turbulent structures from the fan wake with the OGV do not (qualitatively) degrade the shielding of the boundary layer (zooms in Fig. 9). Complementary analysis on the shieding function in the tip gap flow on the same configuration are shown by François *et al.* [6]. They all demonstrate a good robustness and maturity of the approach for turbomachinery flows.

5 VALIDATION AGAINST MEASUREMENTS

Measurements were performed on the selected fan configuration at the studied operating point. Hot-wire measurements in between the fan and the OGV for the three directions of velocity are available. The reader can refer to the paper of Meyer *et al.* [15] for further information.

Journal of Turbomachinery. Received July 06, 2021;
Accepted manuscript posted May 04, 2022. doi:10.1115/1.4054528

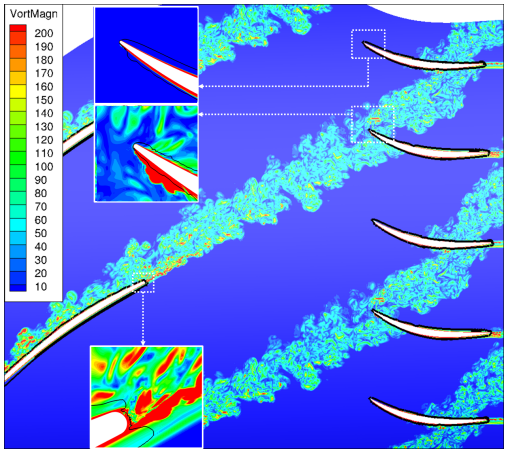

Fig. 9. Visualisation of non-dimensioned vorticity magnitude fields (t_{adim}=2.915 ms) on a developed blade-to-blade surface at 50% of the OGV span. The black lines denote f_d=0.95.

5.1 Aerodynamic performances

	Measurements	Present ZDES	Previous ZDES [6]
Core massflow [kg/s]	6.41	6.43	6.44
Bypass massflow [kg/s]	48.76	48.60	49.26
Bypass pressure ratio	1.108	1.105	1.106

Table 1. Comparison of aerodynamic performances

Table 1 highlights that the aerodynamic performances are retrieved by the present ZDES with a maximum discrepancy lower than 0.4% whereas the previous ZDES [6] exhibits a massflow difference of 1% with the measurements.

5.2 Two-dimensional map visualizations

The ZDES solution has been extracted over a cross-section at HW1 position in order to perform mean flow and wake analyses, by splitting periodic and fully turbulent contributions, and to make comparisons with the latest available measurements. Cyclostationnary axial and tangential velocities are compared between the measurements and the simulation in Fig. 10. A close agreement is obtained on both levels and shape: wakes and tip gap flows are also well retrieved. The depth of the velocity deficit is slightly over-estimated by the simulation. The comparison of the

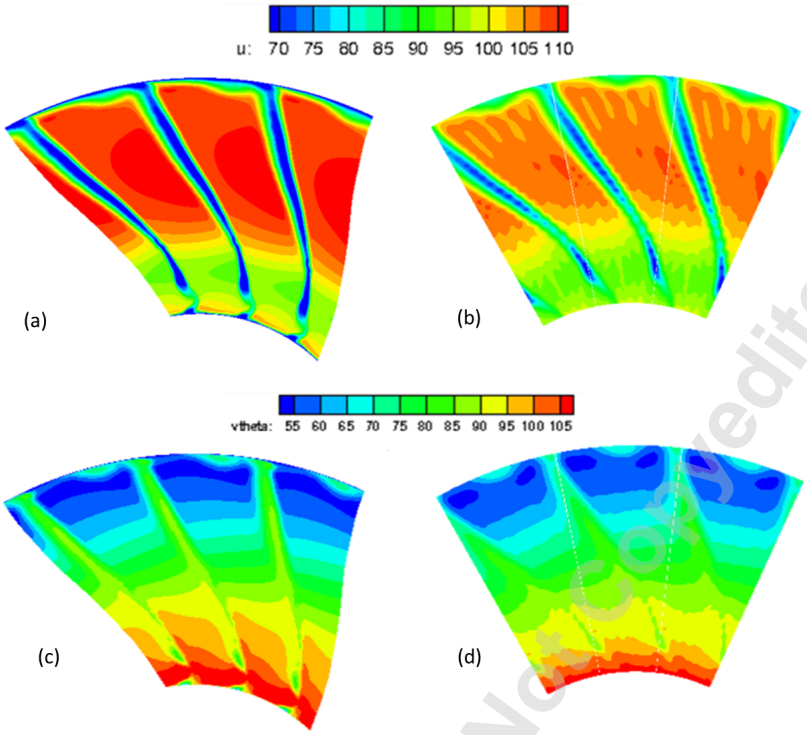

Fig. 10. Maps of velocity flow fields at HW1 plane with ZDES (a-c) and measurements (b-d) - Cyclostationary quantities are shown: axial velocity (a-b) - tangential velocity (c-d). Three blade channels are displayed.)

RMS quantities is shown in Fig. 11. RMS data from the measurements were recalibrated because the hot-wire probes have a cut-off frequency at roughly $8.5\ kHz$. To overcome this difficulty, a 1.5 factor correction, estimated from Parseval identity and integration of velocity PSD up to 8.5 kHz, was applied to the raw measurement data[7]. More details about calibration process are discussed by Polacsek *et al.* [7]. Wakes and tip gap flows are characterized by high values of RMS velocities, visible in the measurements and in the ZDES results. The simulation reproduces quite well the levels and the shape of these turbulent quantities for both velocity components. The tip vortex seems a bit larger in the experiments than in the simulations. In the lower radii part of the map, the flow is solved with URANS with the Spalart-Allmaras model and the RMS velocities cannot be rebuilt. This explains thus the very low values of the RMS quantities in this area, not considered in the comparison. The comparison of the RMS maps hightlights also a noticeable background turbulence present in the measurements although the inlet turbulence is rather low (0.3%). The physical

[7] In the EU project, the same calibration was used by others partners for RMS comparison such as Lewis *et al.* [18] for instance.

Journal of Turbomachinery. Received July 06, 2021;
Accepted manuscript posted May 04, 2022. doi:10.1115/1.4054528

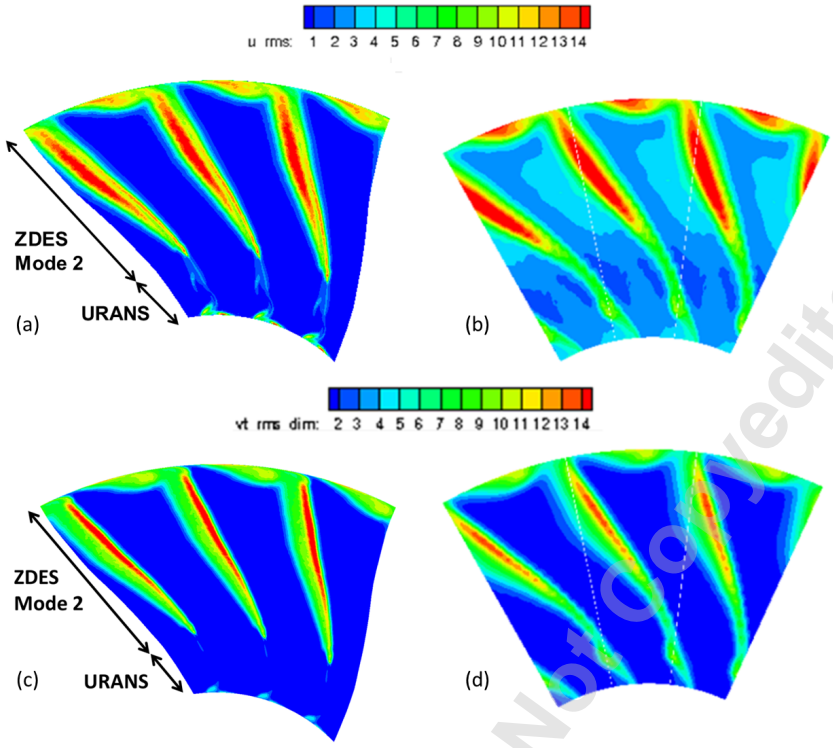

Fig. 11. Maps of axial velocity flow fields at HW1 plane with ZDES (a-c) and measurements (b-d) - RMS quantities are shown: axial velocity (a-b) - tangential velocity (c-d). Three blade channels are displayed.

mechanisms generating this background turbulence are not understood yet. In the simulation, no background turbulence is predicted. Same observations was made by all the partners performing numerical simulations (RANS or LES) in the EU project (see Lewis *et al.* [18] for instance).

5.3 Radial Profiles

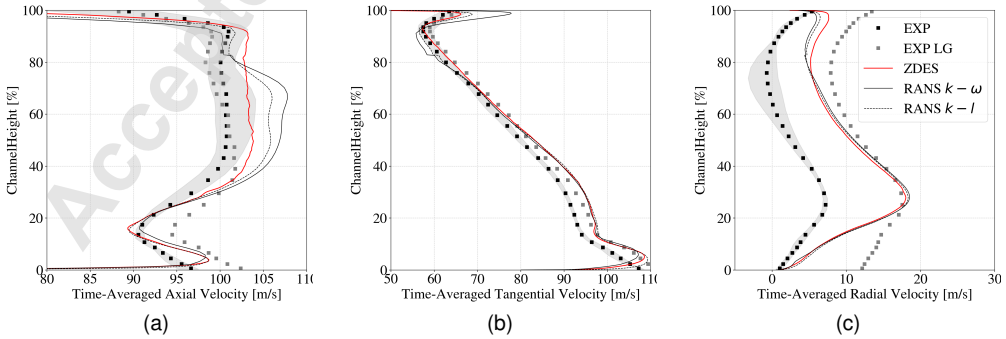

Fig. 12. ZDES and experimental radial profiles at the HW1 location: axial (a), tangential (b) and radial (c) mean velocity

The above 2D fields have been circumferentially averaged in order to perform more quantitative radial profile comparisons. Axial, tangential and radial components of mean velocity provided by ZDES and experiment are plotted in Fig. 12 from left to right, respectively. Measurement data for the same gemeotry with a long-gap between fan and OGV (EXP LG) is also added. The grey area illustrates the uncertainties associated with the measurements between the different inter-channels blades. Indeed, the measured flow is different between adjacent channels. This was observed and referenced in the literature by Meyer *et al.* [15]. According to the authors, the most probable reason are slight geometrical discrepancies between adjacent blades. This is amplified by the aerodynamic flow conditions: for the selected operating point, flow detachment is present on both the fan and the OGV and very small change of stagger angle between adjacent blades may cause these significant differences. Details on the calculation of the error bar are given in the appendix.

Analysis of Fig. 12 shows that mean axial and tangential velocity profile are well retrieved both in shape and levels, the mean axial and tangential velocity being over-estimated by the simulation by less than 3%. The casing boundary layer is not correctly reproduced but the prediction is improved compared to the ZDES from François *et al.* [6] in which the boundary layer was too thin. Concerning the radial velocity, the predicted levels overestimates significantly the measurements ($+5-10\ m/s$). For this flow variable, numerical results of partners in the EU project shows the same trends as the present ZDES results (see Lewis *et al.* [18]). For this reason, measurements on the same fan configuration with a long gap (LG) distance between the fan and the OGV are plotted on the same figure. The ZDES results (such as other numerical results from EU partners of the project) are more consistent with this set of measurements. The difference of measurements between short gap and long gap configurations for this velocity component remain unexplained yet. RANS results using the Menter Shear Stress Transport $k-\omega$ and the Smith $k-l$ models [30,31] are shown on the same figure for comparison using a mesh with five million cells (one rotor and one stator channel). Results are close to the ZDES results for the tangential and the radial velocities but discrepancies are visible on the axial velocity profile ($+6-7\%$). This is attributed to an overestimation of the tip gap flow area at the HW1 position.

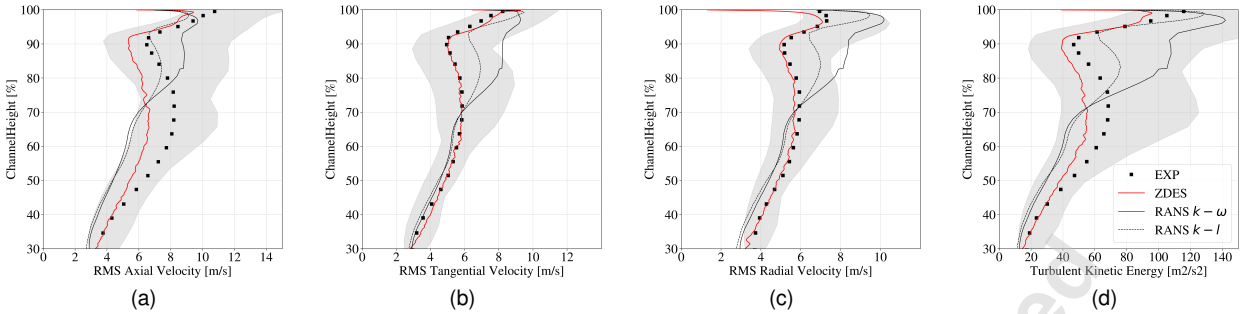

Fig. 13. ZDES and experimental radial profiles at the HW1 location: axial (a), tangential (b), radial (c) RMS turbulent velocity and turbulent kinetic energy (d).

Similar comparisons of radial profiles have been realized for the three RMS components (axial, tangential, radial) of the velocity and the turbulent kinetic energy plotted in Fig. 13. Only the radial section concerning the secondary airflow (ZDES mode 2 solving) is shown. The grey area denotes the uncertainties due to the measurements as mentioned in the previous paragraph, larger for RMS quantities than for mean quantities. For the three components, a sufficiently good agreement is obtained between the measurements and the ZDES results, in particular in the tip gap flow area. In terms of levels, the discrepancies remains within the range of the uncertainties due to the measurements and the shapes of the curves are well reproduced. RANS results, obtained by a reconstruction of the Reynolds tensor with the Boussinesq relation, present larger discrepancies with the measurements than the ZDES results, particularly in the tip gap. The shape of the radial profile is also different from the measurements in this area for the two models.

5.4 Azimuthal Profiles

Comparison of the azimuthal profiles for the cyclostationary velocity is shown in Fig. 14 at 50% and 75% of the duct height to analyse the velocity deficit caused by the wake and at 97% for the tip gap flow. Depth of the velocity deficit[8] and width of the velocity deficit (commonly named wake thickness) are two key parameters in the rotor-stator interaction noise generation for the axial and azimuthal velocity components but they induce a change of incidence on the stator and thus of aerodynamic loading. For these velocity components, the wake thickness is well reproduced by the ZDES simulation compared to the measurements whereas the depth of

[8] for the tangential velocity, this is a peak

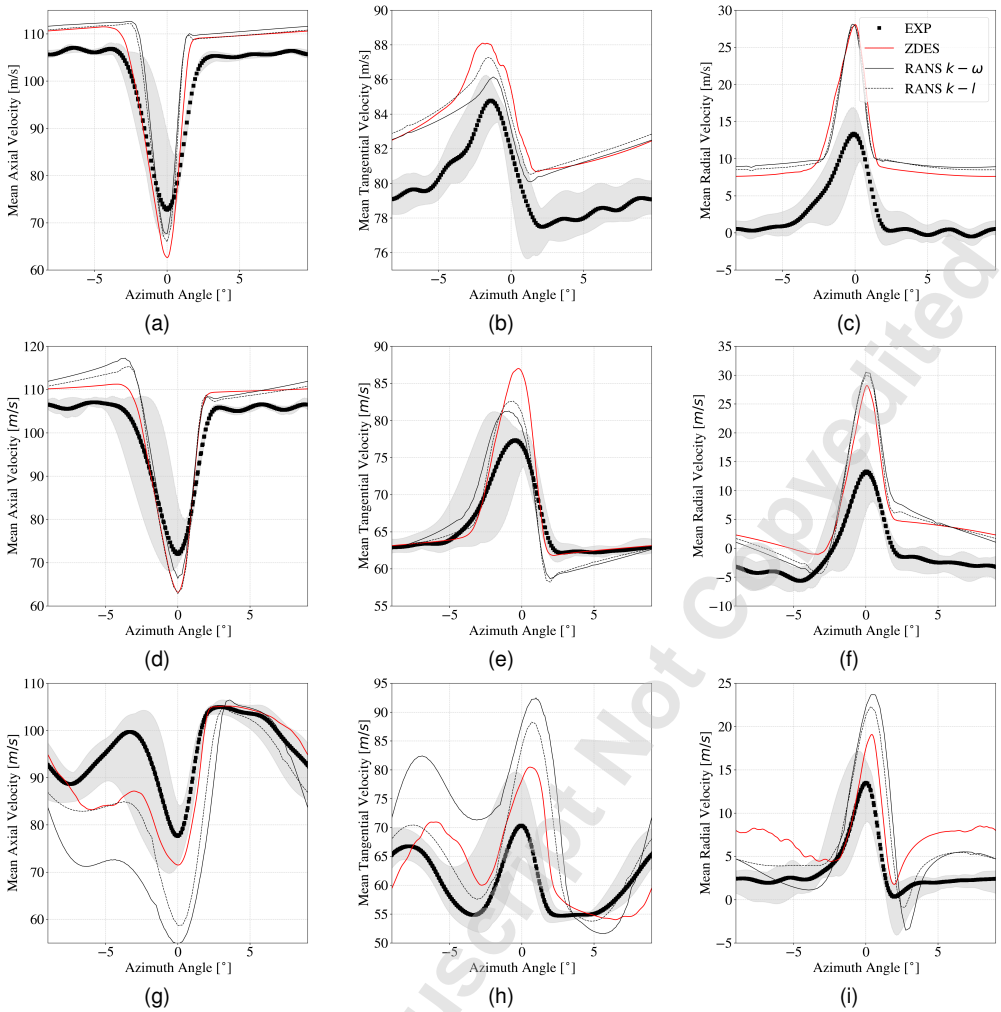

Fig. 14. Experimental, ZDES and RANS azimuthal profiles at the HW1 location for different relative radii: 50% (a-b-c), 75% (g-h-i) and 97% (g-h-i). The three cyclostationary velocity components are displayed: axial (a-d-g), tangential (b-e-h), radial (c-f-i).

the velocity deficit is over-estimated for the relative radii at 50% and at 75% of the duct height by $10-15\%$. RANS results predict also quite well the wake features at 50% and 75% channel height with the same velocity deficit as ZDES but with a smaller width. At 97%, the tip gap flow is visible on the azimuthal profiles with a secondary dip or peak. The main dip/peak and the secondary ones are quite well captured by the ZDES with a slightly lower intensity for the latter one compared to the measurements. Globally, the shape and the levels of the velocity variation over the azimuthal extent are quite consistent between ZDES and measurements. For RANS results, both models tend to overestimate the main dip/peak by factor two. As a consequence, the intensity of the secondary dip/peak is not correct either despite their positions are consistent with

the measurements. Flow angles seem uncorrect with RANS as observed with an overestimation of the axial velocity and an underestimation of the tangential component.

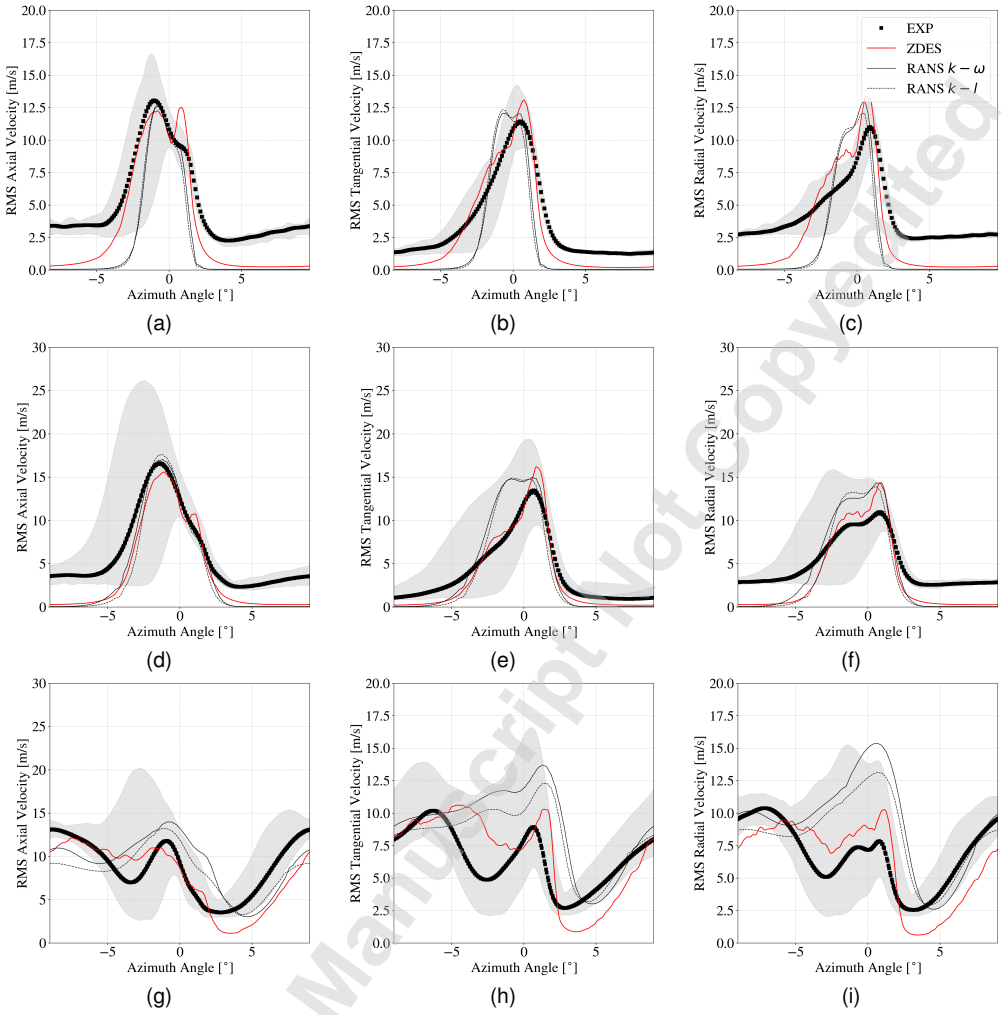

Fig. 15. Experimental, ZDES and RANS azimuthal profiles at the HW1 location for different channel heights: 50% (a-b-c), 75% (d-e-f) and 97% (g-h-i). The three RMS velocity components are displayed: axial (a-d-g), tangential (b-e-h), radial (c-f-i).

RMS velocity component azimuthal profiles depict the repartition of the turbulence energy in the wake and over the three velocity components. This distribution is an important parameter for the broadband rotor-stator interaction noise. Same pattern as Fig. 14 is shown in Fig. 15 for the RMS quantities. At channel height of 50% and 75%, measurements show that the wake exhibits a main peak with an asymmetrical shape or with a secondary peak caused by the flow separation at the fan leading-edge. These features are globally reproduced by the ZDES results except for

some plots with small secondary peaks present in the simulation but absent in the measurements. The width of the wake is very consistent with the measurement while the height of the RMS peak is globally overestimated by 15% in average (from 3% to 25% depending on the plot). The RANS results show always wakes narrower than ZDES and measurements while the height of the RMS peak is quite close to the ZDES results. However, the shape of the RMS profile from RANS results remains often quite symmetrical. For RANS and ZDES, the azimuthal profiles exhibit an absence of turbulence outside the wakes while this turbulence is noticeable in the experiments (mentioned in the analysis of the flow maps in section 5.2). In the tip gap flow, the turbulence is present in the whole inter-blade channel and captured by the simulation (because the tip gap flow fills the whole channel). The variation of the RMS quantities is more complex than at channel height of 50% and 75%: two peaks of similar amplitude are visible. With less accuracy than at mid-height, the shape and the levels of the azimuthal profile are globally reproduced by ZDES : secondary dips/peaks are captured but their positions are shifted and their heights are different compared to the measurements. RANS results show that only a main peak is predicted and RMS levels are overestimated compared to the experimental data.

6 CONCLUSIONS

A Zonal Detached Eddy Simulation approach has been applied to a turbofan stage to simulate the interaction of the turbulent fan wakes with the OGV. The final goal of this simulation is the prediction of the associated broadband noise. Extending the work from François *et al.* [6], the ZDES presented here accounts for a more realistic boundary layer impinging the fan, the simulated massflow rate is closer to the measurements, a better space repartition between the RANS and ZDES mode 2 zones was chosen. To limit the numerical efforts, the number of the OGV blades has been modified to allow a significant reduction of computed inter-blade channels while preserving the main aerodynamic performances.

The ZDES was performed on four revolutions and convergence of the cyclostationnary values (thanks to analysis of numerical controller probes) was achieved. Inspection of the flow field highlights a very consistent behaviour of the shielding function (border between RANS and LES

solving areas) and a correct convection of the broadband turbulent structures to the OGV. The overall analysis of the aerodynamics flow underlines a consistent behavior of the RANS/LES approach applied to a complex turbomachinery flow. The key aerodynamic phenomena responsible for the generation of broadband noise such as the wake interaction in the secondary airflow are qualitatively well captured.

A comparison between the numerical results and a large dataset of hot-wire measurements in between the fan and the OGV using the final calibrations of the project was presented. Global performances (massflow, compression ratio) are better retrieved. Two-dimensional flow maps are well reproduced both in shape and levels by the simulation. Analysis of the radial profiles highlights an excellent agreeement of the RMS quantities between ZDES results and measurements, particularly in the tip gap flow area, while RANS results do not predict consistent radial and azimuthal profiles. Finally, azimuthal profiles comparisons, enabling the inspection of wake thickness and deficit, reveals quite consistent ZDES results with the measurements. These results demonstrate a good maturity of the ZDES approach for complex turbomachinery flows.

The present paper focused only on aerodynamic aspects whereas broadband noise assessment is detailed in the companion paper [2]. This involves complementary turbulent flow analyzes, and sound radiation through dedicated processing methods respectively based on extended Amiet's theory and FWH analogy.

ACKNOWLEDGEMENTS

The presented work was conducted in the frame of the project TurboNoiseBB, which has received funding from the European Union's Horizon 2020 research and innovation programme under grant agreement No. 690714. The authors want to thank the members of the TurboNoiseBB consortium for providing the raw experimental data and for fruitful discussions throughout the project. The authors wish to thank Thomas Node-Langlois from Airbus Civil Aircrafts for providing an experimental dataset in a simplified format ready to use for comparisons with CFD simulations and the inlet aerodynamic profile accounting for the casing boundary layer used in the present simulations. This work was granted access to the HPC resources of CINES under an allocation

made by GENCI (French National Computing Center). The authors are grateful to Sébastien Deck and Nicolas Renard from the Advanced Modeling Turbululence Simulation team in ONERA for the fruitful discussion and their help on the ZDES.

NOMENCLATURE

BC	Boundary Conditions
DDES	Delayed Detached Eddy Simulation
FBP	Fan Blade Passage
HW	Hot-Wire
LE	Leading-edge
OGV	Outlet Guide Vanes
RANS	Reynolds Averaged Navier-Stokes
RMS	Root Mean Square
RSI	Rotor-Stator Interaction
URANS	Unsteady Reynolds Averaged Navier-Stokes
WMLES	Wall-Modeled Large Eddy Simulations
TE	Trailing-edge
ZDES	Zonal Detached Eddy Simulation
f_d	Shielding function in the ZDES

APPENDIX: POSTPROCESSING OF THE EXPERIMENTAL DATA

Meyer *et al.* [15] describes the post-processing of the hot-wire data. Two sets of hot-wire probes allows the measurements of the three components of the velocity at the HW1 plane. A trigger signal from the rotor shaft was recorded with the hot-wire signals. This ensured an exact allocation of each wake to the corresponding blade of the phase downstream of the rotor, allowing to calculate $360°$ phase-averaged flow velocity maps. These flow velocity maps exhibits difference from one channel to an other. Split into 20 subzones (as many as the number of channels), they are averaged and used for comparison with the numerical results (see Fig. 10-b and 10-d). The

RMS quantities are calculated with the RMS value of the instantaneous signal of the velocity for each component. Being different for each channel, they are also averaged (see Fig. 15-b and 15-d).

Experimental uncertainties are quite significant in RMS radial profiles comparison (Fig. 13) and azimuthal profiles comparison (Fig. 14-15). The methodology to calculate these uncertainties is detailled here. First of all, noticeable heterogeneity in the $360°$ flow measurements for the velocity components between the differents fan channels in the HW1 plane are visible [7, 15]. The reason for this heterogeneity is not well understood yet and thus the authors can only make assumptions. Slight fan blade geometry differences (pitch angle, geometry itself) might exist between the adjacent blades. Because the studied operating point in this paper implies a flow separation on the fan leading-edge, small differences of geometry/pitch angle may cause a strong heterogeneity on the appearance/disappearance of flow separation cell in all the blades, on the flow separation cell sizes. This would affect the cyclostationnary flow velocity field downstream of the fan blade at the HW1 measurement plane (Fig. 13) and the turbulence generated in the flow separation cell and then convected, merged with the wake, increasing the variability of the RMS quantities between adjacent channels (Fig. 14-15).

Only this contribution is accounted for in the estimation of the measurement uncertainty presented in aforementionned figures. This estimation proceeds as follows:

1. The $360°$ flow measurements map of velocity is split into 20 subzones,
2. Radial profiles are computed for each subzone,
3. For each radius, the mean, minimum and maximum values are calculated. The mean radial profiles gives the experimental points presented in the comparison plots. The minimum and maximum radial profiles gives the lower and upper bound of the experimental uncertaintities, depicted by the grey area.

The same procedure is applied for the azimuthal profiles.

REFERENCES

[1] Peake, N., and Parry, A. B., 2012. "Modern Challenges Facing Turbomachinery Aeroacoustics". *Annual Review of Fluid Mechanics,* **44**, pp. 227–248.

[2] Polacsek, C., Daroukh, M., François, B., and Barrier, R., 2022. "Zonal Detached Eddy Simulation of the Fan-OGV Stage of a Turbofan Engine: PartII —Broadband Noise Predictions". *Submitted to Journal of Turbomachinery*.

[3] Moreau, A., and Enghardt, L., 2009. "Ranking of Fan Broadband Noise Sources based on an Experimental Parametric Study". In 15th AIAA/CEAS Aeroacoustics Conference (30th AIAA Aeroacoustics Conference), p. 3222.

[4] Deck, S., 2012. "Recent Improvements in the Zonal Detached Eddy Simulation (ZDES) Formulation". *Theoretical and Computational Fluid Dynamics,* **26**(6), pp. 523–550.

[5] Bonneau, V., Polacsek, C., Castillon, L., Marty, J., Gervais, Y., and Moreau, S., 2016. "Turbofan Broadband Noise Predictions using a 3-D ZDES Rotor Blade Approach". In 22nd AIAA/CEAS Aeroacoustics Conference, p. 2950.

[6] François, B., Barrier, R., and Polacsek, C., 2020. "Zonal Detached Eddy Simulation of the Fan-OGV Stage of a Modern Turbofan Engine". Vol. Volume 2A: Turbomachinery of *Turbo Expo: Power for Land, Sea, and Air*. V02AT32A004.

[7] Polacsek, C., Daroukh, M., François, B., and Barrier, R., 2020. "Turbofan Broadband Noise Predictions Based on a ZDES Calculation of a Fan-OGV Stage". In Forum Acusticum, Lyon (France).

[8] Kholodov, P., Koch, R., Sanjosé, M., and Moreau, S., 2021. "Wall-Resolved Large Eddy Simulation of a Realistic Turbofan Rotor for Noise Prediction". In AIAA AVIATION 2021 FORUM, p. 2256.

[9] Leonard, T., Sanjose, M., Moreau, S., and Duchaine, F., 2016. "Large Eddy Simulation of a Scale-Model Turbofan for Fan Noise Source Diagnostic". In 22nd AIAA/CEAS Aeroacoustics Conference, p. 3000.

[10] Arroyo, C. P., Leonard, T., Sanjosé, M., Moreau, S., and Duchaine, F., 2019. "Large Eddy Simulation of a Scale-Model Turbofan for Fan Noise Source Diagnostic". *Journal of Sound*

and Vibration, **445**, pp. 64–76.

[11] Hah, C., and Romeo, M., 2017. "LES Investigation of Wake Development in a Transonic Fan Stage for Aeroacoustic Analysis". In 23rd International Symposium on Air Breathing Engines (ISABE).

[12] Shur, M., Strelets, M., Travin, A., Spalart, P., and Suzuki, T., 2018. "Unsteady simulations of a fan/outlet-guide-vane system: Aerodynamics and turbulence". *AIAA Journal,* **56**(6), pp. 2283–2297.

[13] Suzuki, T., Spalart, P. R., Shur, M. L., Strelets, M. K., and Travin, A. K., 2019. "Unsteady simulations of a fan/outlet-guide-vane system: broadband-noise computation". *AIAA Journal,* **57**(12), pp. 5168–5181.

[14] Casalino, D., Hazir, A., and Mann, A., 2018. "Turbofan Broadband Noise Prediction using the Lattice Boltzmann Method". *AIAA Journal,* **56**(2), pp. 609–628.

[15] Meyer, R., Hakansson, S., Hage, W., and Enghardt, L., 2019. "Instantaneous Flow Field Measurements in the Interstage Section between a Fan and the Outlet Guiding Vanes at Different Axial Positions". In Proceedings of 13th European Conference on Turbomachinery Fluid Dynamics and Thermodynamics, Lausanne, Switzerland, April, pp. 8–12.

[16] Kissner, C., Guérin, S., Seeler, P., Billson, M., Chaitanya, P., Carrasco Laraña, P., de Laborderie, H., François, B., Lefarth, K., Lewis, D., et al., 2020. "ACAT1 Benchmark of RANS-Informed Analytical Methods for Fan Broadband Noise Prediction—Part I—Influence of the RANS Simulation". In Acoustics, Vol. 2, Multidisciplinary Digital Publishing Institute, pp. 539–578.

[17] Guérin, S., Kissner, C., Seeler, P., Blázquez, R., Carrasco Laraña, P., De Laborderie, H., Lewis, D., Chaitanya, P., Polacsek, C., and Thisse, J., 2020. "ACAT1 Benchmark of RANS-Informed Analytical Methods for Fan Broadband Noise Prediction: Part II—Influence of the Acoustic Models". In Acoustics, Vol. 2, Multidisciplinary Digital Publishing Institute, pp. 617–649.

[18] Lewis, D., Moreau, S., Jacob, M. C., and Sanjosé, M., 2021. "ACAT1 Fan Stage Broadband Noise Prediction Using Large-Eddy Simulation and Analytical Models". *AIAA Journal*, pp. 1–

21.

[19] Tucker, P. G., and Wang, Z. N., 2020. "Eddy Resolving Strategies in Turbomachinery and Peripheral Components". *Journal of Turbomachinery,* **143**(1), 12. 010801.

[20] Envia, E., Wilson, A. G., and Huff, D. L., 2004. "Fan Noise: a Challenge to CAA". *International Journal of Computational Fluid Dynamics,* **18**(6), pp. 471–480.

[21] Cambier, L., Heib, S., and Plot, S., 2013. "The Onera elsA CFD Software: Input from Research and Feedback from Industry". *Mechanics & Industry,* **14**(3), pp. 159–174.

[22] Deck, S., Gand, F., Brunet, V., and Ben Khelil, S., 2014. "High-Fidelity Simulations of Unsteady Civil Aircraft Aerodynamics: Stakes and Perspectives. Application of Zonal Detached Eddy Simulation". *Philosophical Transactions of the Royal Society A: Mathematical, Physical and Engineering Sciences,* **372**(2022), p. 20130325.

[23] Riéra, W., Marty, J., Castillon, L., and Deck, S., 2016. "Zonal Detached-Eddy Simulation applied to the Tip-Clearance Flow in an Axial Compressor". *AIAA Journal*, pp. 2377–2391.

[24] Spalart, P. R., Deck, S., Shur, M. L., Squires, K. D., Strelets, M. K., and Travin, A., 2006. "A New Version of Detached-Eddy Simulation, Resistant to Ambiguous Grid Densities". *Theoretical and Computational Fluid Dynamics,* **20**(3), May, p. 181.

[25] Spalart, P., and Allmaras, S., 1992. "A One-Equation Turbulence Model for Aerodynamic Flows". In 30th aerospace sciences meeting and exhibit, p. 439.

[26] Posson, H., and Roger, M., 2007. "Parametric Study of Gust Scattering and Sound Transmission through a Blade Row". In 13th AIAA/CEAS Aeroacoustics Conference (28th AIAA Aeroacoustics Conference), p. 3690.

[27] Hussain, A. K. M. F., and Reynolds, W. C., 1970. "The Mechanics of an Organized Wave in Turbulent Shear Flow". *Journal of Fluid Mechanics,* **41**(2), pp. 241–258.

[28] Gand, F., 2012. "Zonal Detached Eddy Simulation of a Civil Aircraft with a Deflected Spoiler". *AIAA journal,* **51**(3), pp. 697–706.

[29] Verrière, J., Gand, F., and Deck, S., 2016. "Zonal Detached-Eddy Simulations of a Dual-Stream Jet". *AIAA Journal*, pp. 3176–3190.

[30] Menter, F. R., 1994. "Two-Equation Eddy-Viscosity Turbulence Models for Engineering Appli-

cations". *AIAA journal,* **32**(8), pp. 1598–1605.

[31] Smith, B., 1994. "A Near Wall Model for the k-l Two Equation Turbulence Model". In Fluid Dynamics Conference, p. 2386.

LIST OF FIGURES

This section will be created when figures are included with a caption.

LIST OF TABLES

This section will be created when tables are included with a caption.